# MXenes Atomic Layer Stacking Phase Transitions and their Chemical Activity Consequences

José D. Gouveia,[1] Francesc Viñes,[2*] Francesc Illas,[2] José R. B. Gomes[1*]

[1]*CICECO – Aveiro Institute of Materials, Department of Chemistry, University of Aveiro, Campus Universitário de Santiago, Aveiro, Portugal*

[2]*Departament de Ciència de Materials i Química Física & Institut de Química Teòrica i Computacional (IQTCUB), Universitat de Barcelona, c/ Martí i Franquès 1-11, 08028 Barcelona, Spain*

Corresponding authors: jrgomes@ua.pt; francesc.vines@ub.edu

**Abstract:** Two-dimensional (2D) transition-metal nitrides and carbides (MXenes), containing a few atomic layers only, are novel materials which have become a hub of research in many applied technological fields, ranging from catalysis, to environmental scrubber materials, up to batteries. MXenes are obtained by removing the A element from precursor MAX phases, and it is for this reason that it is often assumed that the resulting 2D material displays the MAX atomic layer stacking —an ABC sequence with trigonal ($D_{3d}$) symmetry. By means of density functional theory calculations, including dispersion, this work thoroughly explores the stability of alternative ABA stacking, with $D_{3h}$ hexagonal symmetry, for a total of 54 MXene materials with $M_2X$, $M_3X_2$, and $M_4X_3$ stoichiometries (M=Ti, Zr, Hf, V, Nb, Ta, Cr, Mo, or W; and X=C or N), revealing that for clean MXenes, the ABA stacking is fostered *i*) by the number of *d* electrons in M, *ii*) when X=N rather than X=C, and *iii*) when the surface is terminated by oxygen adatoms. The results suggest that stacking phase transitions are likely to take place under working *operando* conditions, surmounting affordable layer sliding energy barriers, in accordance to the experimentally observed layer distortions in $Mo_2N$. Finally, we tackled the adsorptive and catalytic capabilities implications of such layer phase transition by considering $N_2$ adsorption, dissociation, and hydrogenation on selected ABC and ABA stacked MXenes. Results highlight changes in adsorption energies of up to ~1 eV, and in $N_2$ dissociation energy barriers of up to ~0.3 eV, which can critically change the reaction step rate constant by three to four orders of magnitude for working temperatures in the 400-700 K range. Consequently, it is mandatory to carefully determine the atomic structure of MXenes and to use models with the most stable stacking when inspecting their chemical or physical properties.

## Introduction

Recently, a new class of two-dimensional (2D) materials was discovered by Naguib *et al.* [1] These materials, called MXenes, exhibit high electrical conductivity, hydrophilicity, large surface area, tunable structure, and superior oxidation resistance, among many other properties [2]. Not surprisingly, applications based on MXenes are gaining momentum in areas such as ecofriendly energy [3], greenhouse gases scrubber materials [4,5], batteries [6], water purification [7-9], or heterogeneous catalysis [10], among many other fields of technological applicability. MXenes are usually obtained by selective etching —typically with hydrofluoric acid, HF— of the A element from a precursor MAX phase [11-13]; where M is usually an early transition metal —*e.g.* Ti, Zr, Hf, V, Nb, Ta, Cr, Mo, W—, the A element belongs to a subset of groups XII-XVI of the periodic table, and X is carbon and/or nitrogen [14]. In general, MXenes have $n$+1 layers of hexagonal close-packed transition metals intercalated by $n$ layers of hexagonal close-packed C or N atoms, with a face-centered cubic (*fcc*) —*i.e.* ABC— stacking, and $n$ = 1-3. As a result of the synthesis procedure [1], MXenes feature a surface termination, usually denoted as $T_x$, so that the general formula of MXenes is often expressed as $M_{n+1}X_nT_x$, where $T_x$ is in most cases a mixture of -OH, -O, -H, or -F moieties. Nevertheless, the progress in this field evolves very rapidly and recent HF-free syntheses have been reported yielding MXenes terminated by H and OH only [15,16], or upon fine tuning the layer sequence, reaching thicker $n$ = 5 MXenes, with a central metal layer different from the other ones [17]. Also, even post-synthesis annealing and hydrogenation protocols have been developed to successfully defunctionalize MXene surfaces [5], thus modifying their properties by increasing their electrical conductivity [18].

While MXene surfaces are highly reactive, their atomic structure remains virtually unchanged in the presence of an adsorbate, yet some oddities have been found to occur. For instance, in a computational study, Shao *et al.* [19] predicted that $Mo_2N$ and $W_2N$ MXenes become structurally distorted upon adsorbing a nitrogen molecule. In a recent synthesis and characterization study, $V_2N$ and $Mo_2N$ MXenes were produced by ammonia treatment of the parent carbides [20]. There, the hexagonal phase of $V_2N$ displayed the usual trigonal $D_{3d}$ symmetry of MXenes —in line with an *fcc* ABC stacking—, but the resulting $Mo_2N$ sample was described as having a distorted structure with hexagonal close-packed (*hcp*) $D_{3h}$ symmetry —which would be in line with an ABA stacking. Given the above subtlety, one may wonder if MXene stacking structures other than *fcc* may exist. Another important question concerns whether the transformation from ABC to ABA is intrinsic or can be prompted by either the $T_x$ termination, as suggested on $M_2X$ MXenes with ABA stacking when having O termination, *aka* BiXenes [21], or by the presence of an adsorbate. Both sources of restacking may indeed bestow a symmetry change, eventually translatable into a lowering of the stacking conversion energy

barrier, and, ultimately, prompting a stacking phase transition. Clearly, a deeper analysis regarding the intrinsic stability of the ABC and ABA stacking is needed.

Structural stacking changes may well imply different chemical surface activity, a point than can be key in chemically enhanced few-layered materials. Therefore, information on the preferred stacking of MXenes under working conditions is mandatory to guide future research on the field. However, obtaining this information requires investigating these materials at an inherent atomic level, an aspect difficult to be realized experimentally. Here, motivated by the aforementioned evidence indicating structural distortions and the existence of alternative stackings [19,20], we employ complete and accurate Density Functional Theory (*DFT*) simulations on suited MXene models to systematically analyze the stability of the ABA stacking relative to the usual ABC one. Thus, we consider a wide, organized set of MXenes encompassing different widths, inspecting both thermodynamic and kinetic aspects of the structural conversion. Although the study is mainly focused on pristine MXenes, the possible effect of surface termination on the stability of ABA stacking and/or its conversion is also addressed by considering $T_x$ = O termination, one of the most common ones, and building phase diagrams as a function of oxygen-coverage. Finally, the effect of the ABA stacking on the surface chemical activity of the MXenes is analyzed addressing the textbook $N_2$ adsorption and dissociation steps, key in the technologically relevant Haber-Bosch process of ammonia synthesis [22].

## Computational details

The present study relies on DFT-based first-principles calculations using the Vienna *Ab initio* Simulation Package (*VASP*) [23], carried out on suitable MXene periodic slab models. The calculations were performed within the generalized gradient approximation to the many-body exchange-correlation potential, namely, using the functional developed by Perdew, Burke, and Ernzerhof (*PBE*) [24], augmented with the Grimme D3 method to account for dispersive forces [25], of relevance in the adsorption of $N_2$ and N species on the explored MXenes. The valence electron density was expanded in plane-wave basis sets and the Projector Augmented Wave (*PAW*) method [26] was used to describe the effect of the atomic cores on the valence electronic density. The cutoff for the kinetic energy of the plane waves was set to 415 eV although a higher value of 550 eV was used for the calculation of lattice constants. The convergence criteria for the self-consistent energies and forces on the relaxed structures were set to $10^{-6}$ eV and 0.01 eV·Å$^{-1}$, respectively.

The MXenes studied in the present work were modeled by hexagonal *p*(3×3) periodic supercells containing 9 atoms per layer, see Figure 1. In order to avoid interaction between

MXene replicas due to periodic boundary conditions in the direction perpendicular to the surface, a vacuum region of at least 10 Å was set between periodic copies, both when the surface is clean and when it is $T_x$-terminated. We considered $M_{n+1}X_n$ MXenes, where M is in the Ti, Zr, Hf, V, Nb, Ta, Cr, Mo, W list, X is C or N, and $n$ = 1-3. Only two limit regular stacking possibilities —ABC and ABA— were initially considered, regardless of the MXene width, and thus, neglecting other possible mixed situations, see Figure 1. The calculated lattice parameters, $a$, for the ABC-stacked lattices are in consonance with those reported in the literature [27,28], see Table 1, while the change in $a$ for $n \geq 2$ was found to be lower than 1%; thus, the same lattice constant was used regardless of the MXene thickness. The lattice constants of the ABA-stacked surfaces, however, can vary up to 8% with respect to the ABC situation, the former being smaller than the latter, with the exception of $Mo_2N$. For example, the calculated lattice parameters for ABC- and ABA-stacked $Mo_2C$ are 3.10 Å and 2.84 Å, respectively, in very good agreement with the corresponding values reported by Sun et *al.* of 3.06 and 2.88 Å, respectively [29]. The differences in lattice parameter for each stacking are crucial to obtain accurate, reliable and physically meaningful results, both quantitative and qualitative. Using the example of $Mo_2C$ as a test case, when one uses the same lattice parameter for both stackings, one finds that ABC is more stable, by 0.59 eV per formula unit, while the usage of the proper lattice parameters for each stacking phase yields instead a preference for ABA stacking, by 0.29 eV per formula unit, in very good agreement with previous estimates [29].

The reciprocal space Brillouin zone was sampled using a Monkhorst-Pack 5×5×1 grid of special **k**-points [30]. Convergence tests on **k**-point density and basis set size showed that calculations have a numerical accuracy of about 1 meV per atom. Preliminary tests also showed that spin polarization is required in order to obtain correct total energies for $Ti_2C$, $Zr_2C$, and $Cr_2C$, regardless of their stacking. The saddle-point configurations of the minimum-energy pathways for layer realignments were located *via* the dimer method [31]. Minimum energy and transition state structures were characterized by frequency analysis, with vibrational frequencies obtained within the harmonic approximation upon diagonalization of the corresponding block of the Hessian matrix, whose elements were computed by finite differences of 0.015 Å of analytical gradients. Note that the calculated frequencies were also used to calculate the zero-point energy (ZPE) contribution to the total energy.

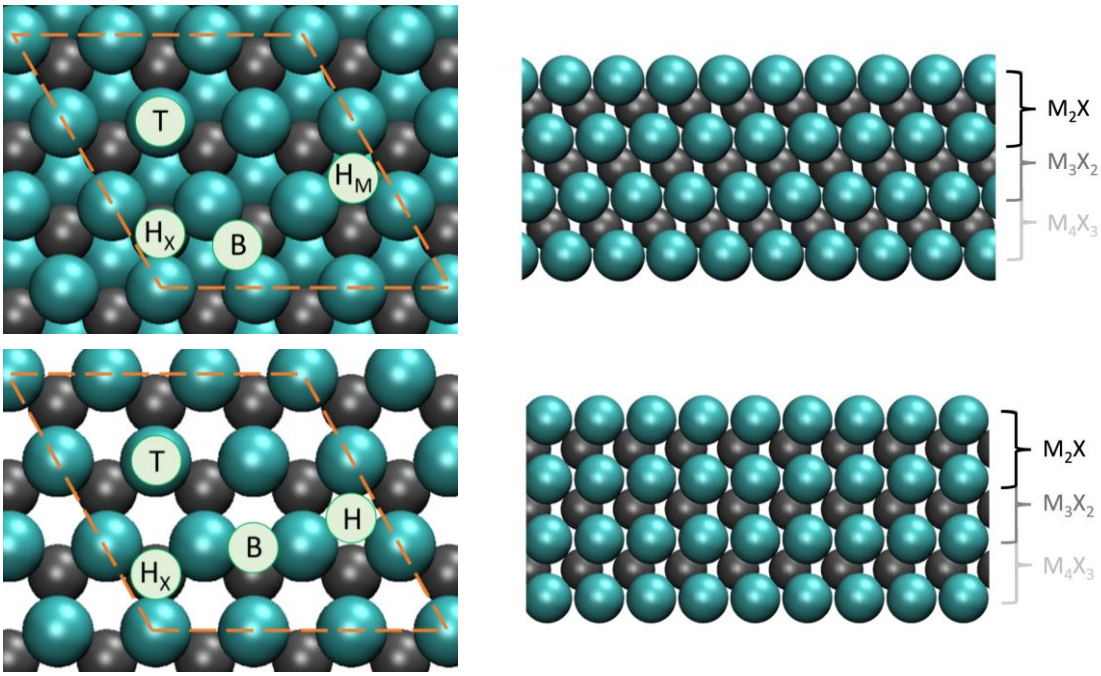


**Figure 1.** Top (left panels) and side (right panels) views of *p*(3×3) MXene supercells. The top images represent ABC stacking, while bottom ones feature ABA stacking. Green (grey) spheres denote M (X) atoms. Tags are shown for high-symmetry relevant surface sites, including bridge (B), top (T), hollow (H), hollow metal ($H_M$), and hollow carbon/nitrogen ($H_X$, in practice $H_C$ or $H_N$) positions. The dashed orange rhombus represents the boundaries of the periodic supercell.

**Table 1.** Calculated lattice parameters, *a*, in Å, for the studied MXenes with ABC (ABA) stacking. Values are given for $M_2X$ MXenes, as they are equivalent for cases with larger *n*.

| ***a*** | ***C*** | ***N*** |
|---|---|---|
| Ti | 3.06 (3.00) | 2.98 (2.86) |
| Zr | 3.27 (3.23) | 3.24 (3.08) |
| Hf | 3.21 (3.16) | 3.17 (3.04) |
| V | 2.90 (2.76) | 2.89 (2.67) |
| Nb | 3.13 (2.94) | 3.15 (2.90) |
| Ta | 3.09 (2.94) | 3.09 (2.88) |
| Cr | 2.82 (2.62) | 2.68 (2.61) |
| Mo | 3.10 (2.84) | 2.79 (2.82) |
| W | 2.88 (2.84) | 2.78 (2.78) |

To take into account the effect of termination, we consider the particular case of oxygen, as aforementioned. To this end, the $O_2$ partial pressure, $p_{O_2}$, *vs.* temperature, *T*, phase diagrams were built by terminating one MXene surface side by O adatoms, and calculating for each $T/p_{O_2}$ pair the Gibbs free energy of adsorption, $G_{ads}$, for a number of O adatoms, $N_O \in [1,9]$, added on the other MXene surface side, and picking the lowest $G_{ads}$ for a given coverage as the ground state. The $G_{ads}$ is calculated as [32]

$$G_{\mathrm{ads}}(T, p_{O_2}) = E_{\mathrm{ads}} - k_{\mathrm{B}}T \ln\left(\frac{Q_{N_{\mathrm{O}}/\mathrm{MXene}}}{(Q_{\mathrm{O}_2})^{N_{\mathrm{O}}/2}}\right) \quad (1),$$

where $E_{\mathrm{ads}}$ is the simultaneous adsorption energy of $N_{\mathrm{O}}$ oxygen adatoms, including the Zero Point Energy (*ZPE*) term, $k_{\mathrm{B}}$ is the Boltzmann constant, $Q_{N_{\mathrm{O}}/\mathrm{MXene}}$ the partition function of the MXene fully terminated by O on one side, and with $N_{\mathrm{O}}$ O adatoms on the other side, and $(Q_{\mathrm{O}_2})^{N_{\mathrm{O}}/2}$ the partition function of $N_{\mathrm{O}}$ oxygen atoms as in gas phase isolated $O_2$ molecules. The adsorption energy of $N_{\mathrm{O}}$ O atoms on a MXene surface, including *ZPE*, is

$$E_{\mathrm{ads}} = \left(E_{N_{\mathrm{O}}/\mathrm{MXene}} + \mathrm{ZPE}_{N_{\mathrm{O}}/\mathrm{MXene}}\right) - E_{\mathrm{MXene}} - \frac{N_{\mathrm{O}}}{2}\left(\mathrm{E}_{\mathrm{O}_2} + \mathrm{ZPE}_{\mathrm{O}_2}\right) \quad (2),$$

where $E_{N_{\mathrm{O}}/\mathrm{MXene}}$ is the total energy of the MXene fully terminated by O on one side and with $N_{\mathrm{O}}$ O adatoms on the other side, $\mathrm{ZPE}_{N_{\mathrm{O}}/\mathrm{MXene}}$ the corresponding *ZPE* term involving $3{\cdot}N_{\mathrm{O}}$ normal vibrational frequencies, $E_{\mathrm{MXene}}$ the total energy of the MXene fully O terminated on only one side, $E_{\mathrm{O}_2}$ the total energy of an $O_2$ molecule, and $\mathrm{ZPE}_{\mathrm{O}_2}$ the *ZPE* term for its stretching vibrational mode. Notice that the DFT overestimation of the binding energy of $O_2$, here estimated to be of 0.93 eV compared to experimental values [33], has not been corrected to deliver DFT-consistent results, and more reliable estimates would imply O adatom binding energy reduced by half the aforementioned value. The $N_{\mathrm{O}}$/MXene partition function is

$$Q_{N_{\mathrm{O}}/\mathrm{MXene}} = \prod_i \frac{1}{1-\exp\left(\frac{-h\nu_i}{2k_{\mathrm{B}}T}\right)} \quad (3),$$

where $\nu_i$ are the $3{\cdot}N_{\mathrm{O}}$ normal vibrational frequencies of the $N_{\mathrm{O}}$ O adatoms. The partition function of the $O_2$ molecule in gas phase is the product of vibrational, rotational, and translational contributions, $Q_{\mathrm{O}_2} = q_{\mathrm{vib}} \cdot q_{\mathrm{rot}} \cdot q_{\mathrm{trans}}$, where the vibrational contribution is computed in the same way as $Q_{N_{\mathrm{O}}/\mathrm{MXene}}$ albeit involving one vibrational frequency only; the rotational partition function is

$$q_{\mathrm{rot}} = \frac{T}{2\theta_{\mathrm{O}_2}} \quad (4),$$

where $\theta_{\mathrm{O}_2}$ is the rotational temperature of the $O_2$ molecule, calculated from the diagonalization of its inertia tensor, and the translational partition function is

$$q_{\mathrm{trans}} = \left(\frac{2\pi m_{\mathrm{O}_2} k_{\mathrm{B}}T}{h^2}\right)^{3/2} \frac{k_{\mathrm{B}}T}{p_{O_2}} \quad (5),$$

where $m_{\mathrm{O}_2}$ is the mass of one $O_2$ molecule.

## Results and discussion

Let us first assess the stability of ABA stacking relative to the ABC one for the explored 54 MXenes. Table 2 reports the calculated values and Figure 2 provides the corresponding plots of the energy difference per MXene formula unit, $\Delta E_{stack} = E_{ABA} - E_{ABC}$, for X= C, N and for the different *n* values. Negative values indicate that the ABA stacking is preferred, and values close to zero correspond to near-degeneracy between the two stacking configurations. For the $M_2X$ stoichiometry ($n$ = 1), all group VI MXenes and group V nitrides but $V_2N$ either prefer ABA stacking or both stackings are found to be nearly equally stable. This prediction is in agreement with experiments indicating that $V_2N$ exhibits the ABC stacking [20]. On the remaining $M_2X$ surfaces, the ABC stacking is clearly preferred. Note also that $\Delta E_{stack}$ is smaller by at least several tenths of eV on each $M_2N$ than on its corresponding $M_2C$ MXene, with the sole exception of $W_2X$, where the order of stability is actually reversed. In the case of $M_3X_2$ ($n$ = 2) or $M_4X_3$ ($n$ = 3) the stacking preferences on group VI are maintained with respect to the thinner MXenes, although ABA stacking becomes the most stable for $V_3N_2$ and $V_4N_3$.

For all of the M/X combinations, $\Delta E_{stack}$ appears to vary linearly with *n*. For the $d^2$ MXenes and $d^3$ carbides, $\Delta E_{stack}$ increases by *circa* 1 eV per M-X layer per formula unit, meaning that the addition of more layers further stabilizes the ABC stacking. On the $d^4$ MXenes and $d^3$ nitrides, the opposite holds, and ABA becomes more stable by an average of around 0.49 eV per formula unit per added layer. The sole exception to this trend are the aforementioned vanadium nitride MXenes, as the ABC stacking is favored for $V_2N$, but ABA becomes stabilized by around 0.26 eV per formula unit per V-N layer, which is enough to change the sign of $\Delta E_{stack}$, from 0.23 eV on $V_2N$, to the nearly degenerate -0.02 eV on $V_3N_2$, to -0.30 eV on $V_4N_3$. The $W_{n+1}C_n$ MXenes display the greatest preference towards ABA, with this stacking becoming ~1 eV more advantageous per formula unit per added W-C layer. In summary, the rule of thumb is that each type of MXene releases/absorbs a fixed amount of energy per realigned layer, so that an increase in *n* usually maintains the stacking preference, reinforcing its energetic preference.

**Table 2.** Energetic difference per formula unit, $\Delta E_{stack}$, in eV, between ABC and ABA stacking on all the studied 54 pristine (leftmost numeric columns) or oxygen-terminated (rightmost collumns) MXenes. Bold font indicates energetic preference for ABA stacking, or a nearly degenerate state in between ABC and ABA.

| X | M | $M_2X$ | $M_3X_2$ | $M_4X_3$ | $M_2XO_2$ | $M_3X_2O_2$ | $M_4X_3O_2$ |
|---|---|---|---|---|---|---|---|
| **C** | **Ti** | 1.24 | 2.51 | 3.71 | 1.18 | 1.82 | 3.20 |
| | **Zr** | 1.46 | 2.68 | 3.91 | 1.45 | 2.20 | 3.70 |
| | **Hf** | 1.58 | 2.90 | 4.27 | 1.61 | 2.31 | 3.93 |
| | **V** | 0.88 | 2.00 | 2.73 | 0.59 | 0.76 | 1.48 |
| | **Nb** | 0.69 | 1.46 | 2.15 | 0.96 | 1.19 | 1.95 |
| | **Ta** | 0.84 | 1.67 | 2.63 | 0.99 | 1.17 | 1.90 |
| | **Cr** | **0.00** | **0.01** | **-0.27** | **-1.05** | **-1.49** | **-1.85** |
| | **Mo** | **-0.29** | **-0.60** | **-1.05** | **-1.52** | **-2.37** | **-2.95** |
| | **W** | **-0.46** | **-1.34** | **-2.56** | **-2.33** | **-3.51** | **-4.69** |
| **N** | **Ti** | 0.90 | 1.64 | 2.50 | 0.87 | 0.78 | 1.52 |
| | **Zr** | 0.84 | 1.47 | 2.31 | 1.06 | 1.10 | 1.89 |
| | **Hf** | 0.89 | 1.59 | 2.55 | 1.15 | 1.17 | 1.97 |
| | **V** | 0.23 | **-0.02** | **-0.30** | **-0.01** | **-0.37** | **-0.76** |
| | **Nb** | **-0.03** | **-0.53** | **-0.95** | **0.04** | **-0.54** | **-0.78** |
| | **Ta** | **-0.19** | **-0.81** | **-1.52** | **-0.01** | **-0.78** | **-1.21** |
| | **Cr** | **-0.19** | **-0.88** | **-1.53** | **-1.13** | **-1.72** | **-2.32** |
| | **Mo** | **-0.29** | **-0.77** | **-1.09** | **-1.28** | **-1.49** | **-1.90** |
| | **W** | **-0.38** | **-0.86** | **-1.10** | **-1.30** | **-1.42** | **-1.89** |

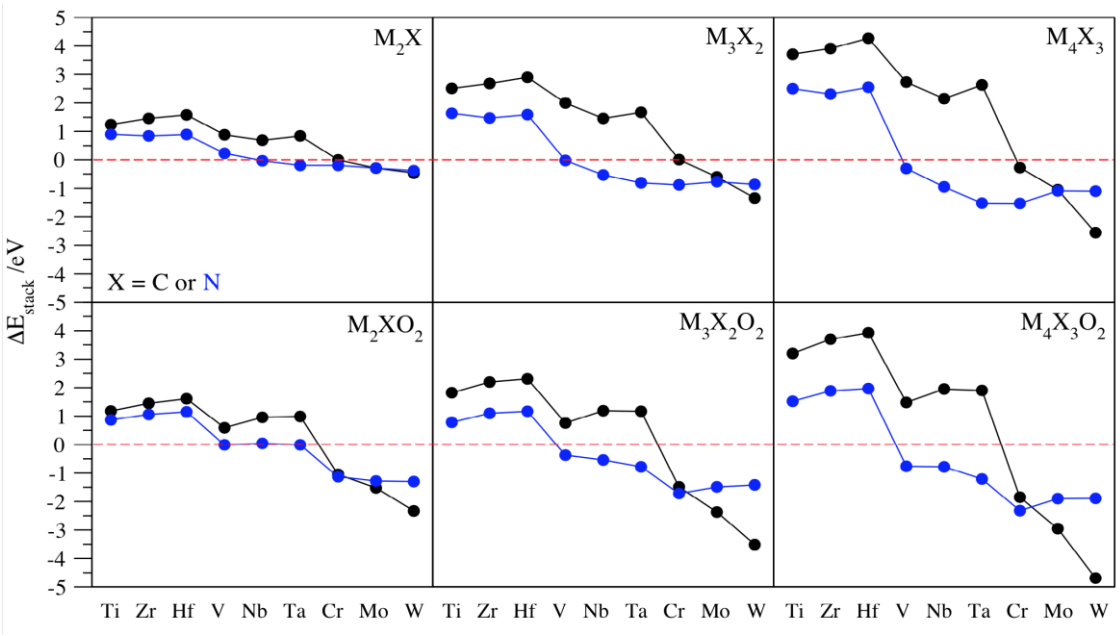


**Figure 2.** Plots of $\Delta E_{stack}$ as a function of the M element for several MXene widths, *n*, X compositions —C in black, N in blue—, with and without O termination. The dashed red line denotes the equal energetic stability of ABC and ABA stacking, with negative values indicating preference for the latter.

The above trends are very similar when the MXene surfaces are terminated by oxygen, but generally considerably strengthening the ABA stacking, as shown in Table 2 and Figure 2. In fact, nearly all $\Delta E_{stack}$ values for the O-terminated MXenes in Table 2 are smaller than those of clean systems. As seen in Figure 2, the O-termination greatly stabilizes ABA stacking on group VI $M_{n+1}X_nO_2$ MXenes, with $\Delta E_{stack}$ becoming even more negative, by differences between -0.79 to -2.17 eV per formula unit. Note, however, that the formula unit is different for each stoichiometry and, hence, comparison should be restricted to a given family of MXenes. From this energetic analysis it becomes clear that the ABA stacking preference is enhanced when *i)* the number of *d* electrons of the metal increases, *ii)* N is present instead of C, *i.e.* the number of X *p* electrons increases, and/or *iii)* the MXenes are O-covered, regarded as an electron-rich $T_x$ termination, altogether suggesting that ABA stacking is fostered by a higher electronic density of the material. These conclusions are in line with the experimentally observed possible ABA stackings on $Mo_2N$ [20], and the previously reported ABA energetic preferences for $Mo_2C$ [29], or the distortions reported on $Mo_2N$ and $W_2N$ [19]. Note also that, although the present results corroborate the stability of ABA $Mo_2C$ or $Mo_2CO_2$ on the hydrogen evolution reaction, as posed by Lv and coworkers [21], their proposal of preferential ABA stacking for $Ti_2C$, $Nb_2C$, $V_2C$, and $Ti_3C_2$ —or their O-terminated versions, $Ti_2CO_2$, $Nb_2CO_2$, $V_2CO_2$, and $Ti_3C_2O_2$— is not supported by the present calculated data. Even though such structures have been proven to be

dynamically stable over 3 ps *ab initio* molecular dynamics runs, the present results clearly show that, for these MXenes, the ABC stacking phases are energetically favorable so that long enough molecular dynamics runs would eventually lead to the lowest ABC structure.

A critical point here is whether the adoption of an ABA stacking would be kinetically inhibited, especially when such MXenes are generated from ABC-stacked MAX phases. In order to address the possible kinetic inhibition for the ABC→ABA phase transition, the conversion energy barriers, $E_b$, were calculated for the MXenes which displayed energetic preference towards ABA, *i.e.* $\Delta E_{stack} < 0$. The corresponding values for pristine $M_nX_{n+1}$ MXenes are reported in Table 3. For $n$ = 1, the mechanism involves only a simple C→A sliding. However, for $n \geq 2$, the transition from ABC to ABA may occur in several steps, involving the lateral sliding of a single or a few layers, with many local minima with regions of coexistence of ABC and ABA stacking. A careful examination of the sliding mechanism was carried out, guided by the found trends that the slide of surface metal layers is easier than the inner ones. The $E_b$ values shown in Table 3 correspond to the highest energy barrier among all the considered steps of the given found mechanism, whose respective slide acts as the rate-limiting energy step. Figure 3 shows examples for $n$ = 1-3; $W_2C$, $W_3C_2$, and $W_4C_3$, showing a guide to all the contemplated sliding steps, given that other MXenes follow similar mechanisms.

Let us analyze the exemplary $W_2C$, $W_3C_2$, and $W_4C_3$ cases in fine detail. On $W_2C$, the transition from ABC to ABA stacking (top row of Fig. 3) implies a single exothermic step. On $W_3C_2$, the ABCAB transition to ABABA stacking (middle row of Fig. 3) implies three exothermic steps; the first two align the outer W layers with the inner one, while the last one aligns the remaining C layers with each other. Lastly, the $W_4C_3$ transition from ABCABCA to ABABABA stacking comprises five steps (bottom row of Fig. 3); the first two are exothermic and align an outer W layer and its adjacent C layer with the inner closer W and C layers, respectively. The third step is highly exothermic, $\Delta E$ = -1.08 eV per $W_4C_3$ unit, and aligns the other outer W layer with its closest W layer. After this step, the stacking is CACABAB, which is none other than two ABA-stacked $W_2C$ surfaces glued by a layer of carbon. This stacking is very stable and, for this reason, the step that follows, that is, the sliding of the first outer W layer to become aligned with the two farthest W layers is endothermic, $\Delta E$ = 0.48 eV per $W_4C_3$ unit, making this the highest-barrier step in the process, with an $E_b$ of 1.12 eV per $W_4C_3$ unit. The last step aligns the last W layer with the other three, and the final ABABABA stacking is achieved, with a global $\Delta E_{stack}$ of -2.56 eV per $W_4C_3$ unit. Note that the sliding of the outer W layers normally implies low $E_b$ values, in between 0.49 and 0.62 eV per $W_4C_3$ unit, whereas the inner W or C layers slides require surmounting larger $E_b$ values, between 0.69 and 1.10 eV, again per $W_4C_3$ unit. The sole exception is the aforementioned realignment of the outer W layer in $W_4C_3$,

as here the outer $E_b$ of 1.12 eV per $W_4C_3$ unit is clearly biased by the positive $\Delta E$ = 0.48 eV per $W_4C_3$ unit, likely due to the breaking of two C-glued ABA $W_2C$ units.

From the values in Table 3, it is clear that the ABC→ABA conversion is actually not inhibited at all in many cases (see *e.g.* the $Mo_2N$, $Mo_3N_2$, and $W_2N$ cases, with $E_b$ values of 0.12 eV per formula unit), and a rapid conversion towards the energetically more stable ABA stacking is to be expected, although one has to keep in mind that nucleation and phase boundary expansion has not been considered here, given the limitations of the employed methodology. The global observed trend is that the phase transition energy barrier increases with the MXene thickness, *i.e.* with *n*, surpassing 1 eV per formula unit on $M_4C_3$ and $W_3C_2$. Interestingly, while the $W_{n+1}C_n$ family displays the largest preference for ABA stacking among all MXenes, $W_3C_2$ and $W_4C_3$ also exhibit some of the highest energy barriers to reach that atomic structure, suggesting a possible kinetic hindrance. Nevertheless, the energy barrier values are not as high as to become insurmountable at working catalytic *operando* conditions between 400 and 700 K although the time scale may be an issue.

**Table 3.** Calculated ABC→ABA stacking phase transition energy barriers, $E_b$, in eV per formula unit, for the studied $M_{n+1}X_n$ MXenes.

| $E_b$ | $M_{n+1}C_n$ | | | $M_{n+1}N_n$ | | |
|---|---|---|---|---|---|---|
| ***n*** | **1** | **2** | **3** | **1** | **2** | **3** |
| **Ti** | — | — | — | — | — | — |
| **Zr** | — | — | — | — | — | — |
| **Hf** | — | — | — | — | — | — |
| **V** | — | — | — | — | 0.72 | 0.91 |
| **Nb** | — | — | — | 0.64 | 0.54 | 0.72 |
| **Ta** | — | — | — | 0.53 | 0.52 | 0.70 |
| **Cr** | 0.72 | 0.88 | 1.04 | 0.33 | 0.32 | 0.69 |
| **Mo** | 0.52 | 0.93 | 1.22 | 0.12 | 0.12 | 0.51 |
| **W** | 0.49 | 1.10 | 1.12 | 0.12 | 0.26 | 0.77 |

To investigate the effect of the surface termination on the relative kinetic stability of ABC and ABA stackings, we consider the case where both sides of the surfaces are fully covered by oxygen. The $E_b$ values for the ABC→ABA phase transition on O-terminated MXenes are encompassed in Table 4, and are, generally, lower than on the pristine MXene counterparts, as one might well predict regarding the enhanced energetic preference towards ABA, as observed in Table 2. In the case of $M_2XO_2$, the phase transition generally involves two steps: the realignment of the M/X layers from ABC to ABA, and the posterior repositioning of the O atoms into their ground state adsorption site —$H_X$ on nearly all MXenes. The exception to the general trend is $W_2NO_2$, which prefers a mixed structure with one layer of O on $H_N$ and with the other O layer on an H site, *cf.* Figure 1. For comparative purposes, the values shown in

Table 4 refer to the highest energy barrier per formula unit among the steps of the realignment of the M/X layers only. Nevertheless, in general terms, the energy barriers for surface O relocation are rather high, between 0.5 and 1.1 eV per formula unit, yet still surmountable depending on the *operando* conditions, see the example of $Cr_2CO_2$ in Figure 4. Comparing the $E_b$ values of Tables 3 and 4, one readily notices that the O-termination usually reduces the energy barriers by a few tenths of eV. This is understandable, as the presence of O on the surface weakens the bonds between the outer metal atoms and the inner X layer atoms, allowing for energetically easier layer sliding. On $Mo_2NO_2$, the realignment barrier is only 0.12 eV per formula unit. This, together with the relative energetic stability, 1.28 eV per formula unit in favor for ABA stacking, further justifies the experimental observation of a nitride phase with a different layer stacking than the precursor.[20]

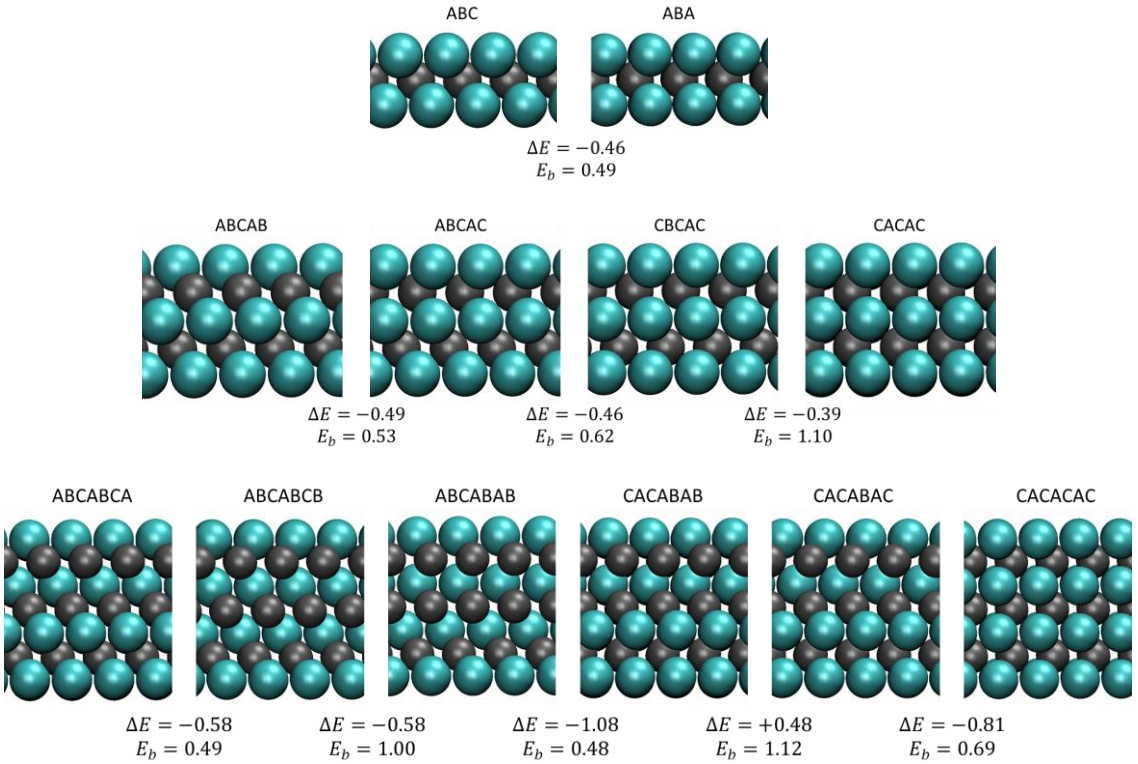


**Figure 3.** Side views of the sliding steps taken by the $W_2C$ (top), $W_3C_2$ (middle), and $W_4C_3$ (bottom) MXene surfaces in their transition from ABC to ABA stacking. Below each transition step, the values of the reaction step energy change, ΔE, and its energetic barrier, $E_b$, are given in eV and per formula unit.

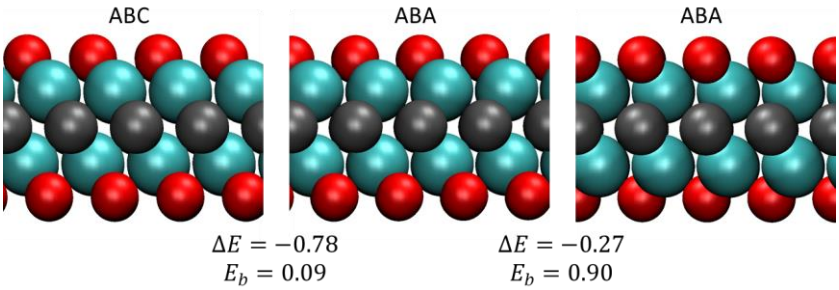


**Figure 4.** Side view of the sliding steps taken by $Cr_2CO_2$ MXene surface during its ABC→ABA stacking transition. Below each transition step, the values of the reaction step energy change, ΔE, and its energetic barrier, $E_b$, are given in eV.

**Table 4.** Calculated ABC→ABA stacking phase transition energy barriers, $E_b$, in eV per formula unit, for the studied fully O-covered $M_{n+1}X_nO_2$ MXenes. The listed values refer to the highest energy barrier, given per formula unit, among all the sliding realignment steps of the M/X layers only.

| $E_b$ | $M_{n+1}C_nO_2$ | | | $M_{n+1}N_nO_2$ | | |
|---|---|---|---|---|---|---|
| ***n*** | **1** | **2** | **3** | **1** | **2** | **3** |
| Ti | — | — | — | — | — | — |
| Zr | — | — | — | — | — | — |
| Hf | — | — | — | — | — | — |
| V | — | — | — | 0.53 | 0.59 | 0.71 |
| Nb | — | — | — | 0.54 | 0.55 | 0.67 |
| Ta | — | — | — | 0.39 | 0.45 | 0.52 |
| Cr | 0.09 | 0.55 | 0.72 | 0.13 | 0.12 | 0.44 |
| Mo | 0.44 | 0.70 | 0.92 | 0.12 | 0.11 | 0.30 |
| W | 0.25 | 0.86 | 0.91 | 0.10 | 0.13 | 0.53 |

Given the low $E_b$ per formula unit values here reported for a series of cases, one may wonder whether O adsorption could be enough to drive the stacking phase transition. This is exemplified on the $W_2N$ system, which has been theoretically predicted to yield a $D_{3h}$ ABA symmetry [19]. We begin this analysis by covering its *p*(3x3) supercell with O adatoms on $H_M$ sites —the most stable sites for O adsorption— while the other side is sequentially saturated by O. The simultaneous adsorption energy per oxygen atom, $E_{ads}/N_O$, was calculated as detailed above, and the stepwise O adsorption, $E_{ads}^{step}$, addressing the MXene continuous oxidation process was obtained as well, as

$$E_{ads}^{step} = E_{N_O/MXene} - E_{N_O-1/MXene} - \frac{E_{O_2}}{2} \quad (6).$$

The $E_{ads}^{step}$ value gives information on the energy released when an MXene containing $N_O - 1$ O adatoms adsorbs an additional O atom. The $E_{ads}/N_O$ and $E_{ads}^{step}$ values are

encompassed in Table 4, for $W_2N$ in either an ABC or an ABA configuration. On the one hand, the values of $E_{ads}/N_O$ in Table 5 are all negative, implying exothermicity, at least until full O coverage, with values ranging from -3.56 to -5.08 eV for ABC stacking, and varying much less, between -4.07 and -4.27 eV, for ABA stacking. On the other hand, the $E_{ads}^{step}$ values are always negative as well, but on ABC stacking largely oscillate between -1.67 eV and -7.09 eV. Such fringe situations can be understood when the system symmetry is accounted for as $N_O$ increases. Indeed, the stepwise adsorption is stronger whenever the symmetry is reduced from $C_{3v}$ to $C_{1h}$ by adsorbing the extra O atom. This situation is not observed on the ABA stacking, with $E_{ads}^{step}$ values ranging between -3.69 and -4.30 eV, as the surface is kept intact during the O coverage.

**Table 5.** Adsorption energy per O atom, $E_{ads}/N_O$, and stepwise adsorption energy, $E_{ads}^{step}$, on the $W_2N$ MXene with ABC or ABA stacking configurations.

| $N_O$ | ABC | | | ABA | |
|---|---|---|---|---|---|
| | Symmetry | $E_{ads}/N_O$ | $E_{ads}^{step}$ | $E_{ads}/N_O$ | $E_{ads}^{step}$ |
| 0 | $C_{3v}$ | ---- | ---- | ---- | ---- |
| 1 | $C_{3v}$ | -3.56 | -3.56 | -4.24 | -4.24 |
| 2 | $C_{1h}$ | -5.08 | -6.59 | -4.27 | -4.30 |
| 3 | $C_{3v}$ | -4.02 | -1.92 | -4.24 | -4.18 |
| 4 | $C_{1h}$ | -4.79 | -7.09 | -4.23 | -4.20 |
| 5 | $C_{1h}$ | -4.19 | -1.78 | -4.20 | -4.07 |
| 6 | $C_{3v}$ | -3.77 | -1.67 | -4.19 | -4.12 |
| 7 | $C_{1h}$ | -3.89 | -4.60 | -4.15 | -3.94 |
| 8 | $C_{3v}$ | -3.69 | -2.35 | -4.11 | -3.86 |
| 9 | $D_{3d}$ | -3.58 | -2.62 | -4.07 | -3.69 |

The strongest $E_{ads}^{step}$ values are associated to a surface relaxing effect observed on the MXene surface. As shown in Figure 5 for the initial O adsorptions with $N_O$ = 0-2, when the symmetry is $C_{1h}$, the lattice becomes largely distorted, and the apparent stronger $E_{ads}^{step}$ = -6.59 eV is not due solely to the O adsorption itself, but in part due to the surface relaxation it promotes. The symmetry reduction caused by the adsorption seems to already reduce the energy barrier required by the $W_2N$ surface to relax into a more stable configuration. This explains the oscillation between small and large $E_{ads}^{step}$ alongside the $C_{3v}$ and $C_{1h}$ symmetries. This conclusion was confirmed by repeating the calculations, but breaking the symmetry of the system, making it $C_1$. Similar oscillations to the ones in Table 2 were obtained, yet for the last O adsorption, an $E_{ads}^{step}$ of very high absolute value of -12.77 eV was obtained, not corresponding to the sole O

adsorption, but being mostly the result of the MXene layer realignment upon conversion of the ABC stacking into the ABA one, highlighting how the strong O adsorptions are enough to surmount the almost insignificant $E_b$ values. Note that the positions occupied by the O atoms are not the same on both sides of the MXene after the transition to ABA: O is placed over H sites on one side, and over $H_N$ sites on the other side, see Figure 6, in line with the above results. This placement of the O atoms is preferred over pure $H_N$ or H by 0.05 and 0.54 eV per unit supercell, respectively.

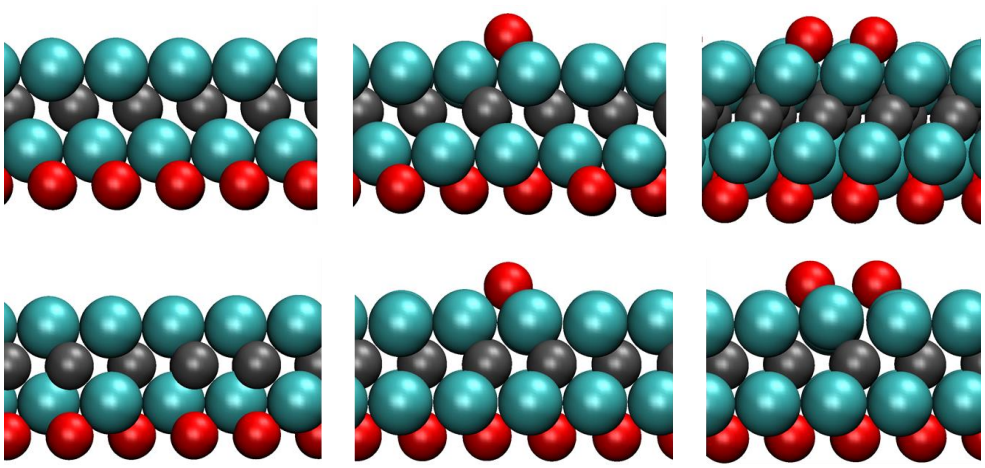

**Figure 5.** Side views of the optimized $W_2NO_x$ MXene (0001) surface, with ABC (top) or ABA (bottom) stacking, and with $N_O = 0$ (left), $N_O = 1$ (middle), both with $C_{3v}$ symmetry, and $N_O = 2$ (right), with $C_{1h}$ symmetry. Note the severe surface distortion that occurs when $W_2N$ with ABC stacking and one surface fully O-covered, adsorbs two O atoms on the other side.

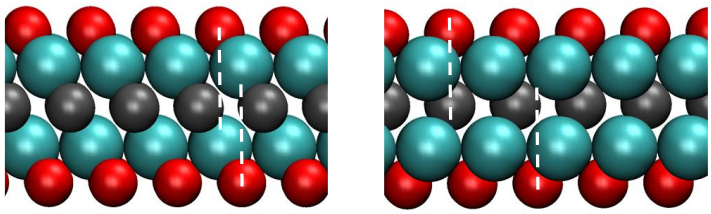

**Figure 6.** Side views of a $W_2NO_2$ MXene surface with ABC (left) and ABA (right) stacking. Dashed lines are guides to the eye; notice the asymmetry of the hollow sites occupied by the O atoms in the case of ABA.

Following the previous discussion, the question of whether ABA stacking is more stable for any O coverage arises. From Figure 2, it is clear that the ABA stacking is more favorable for $W_2N$ both as pristine and fully O-covered, and the small $E_b$ of the pristine $W_2N$ of 0.12 per formula unit would indicate that the energetic release by the adsorption of a moiety would actually be enough to overcome such a barrier. To further illustrate this point, the calculated

$T/p_{O_2}$ phase diagram of oxygen coverage of $W_2N$ is shown in Figure 7. Each point of the diagram displays the situation with lowest $G_{ads}$. This is exemplified *e.g.* on the left panel of this Figure for a fixed pressure of 1 bar ($10^5$ Pa), and different surface O coverage situations as a function of the temperature. Inspection of Figure 7 reveals that an O-free situation at 1 bar is only attainable at an extreme $T$ above ~2200 K. The transition region between the fully O-covered situation, and the pristine MXene is very narrow, as seen in the phase diagram of Figure 7, and one should regard such MXenes as O-covered at normal $O_2$ partial pressures, yet O-free surfaces are attainable at ultra-high-vacuum conditions and high temperatures, *e.g.* below $10^{-8}$ Pa and $T$ ~800 K, although there exist O-cleaning protocols by annealing and hydrogenation steps [5].

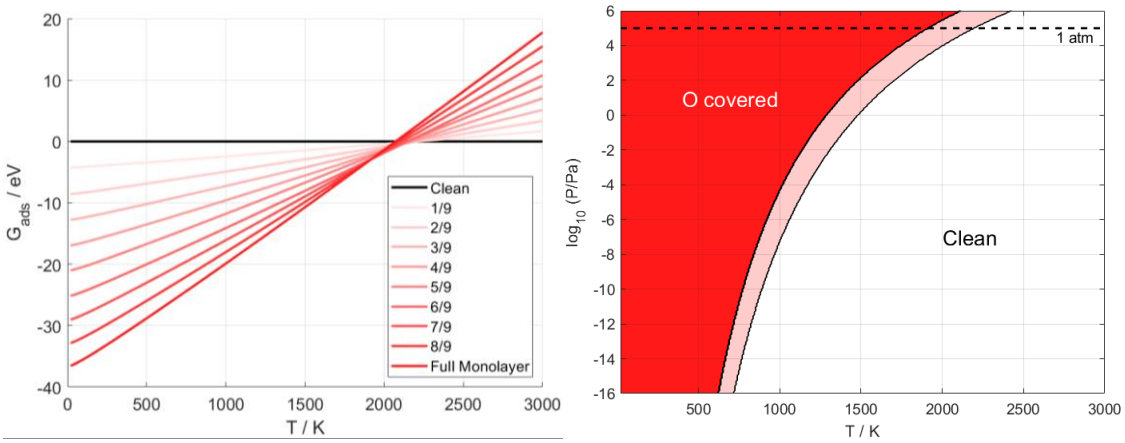


**Figure 7.** Gibbs free adsorption energies, $G_{ads}$, as a function of temperature, $T$, for each fraction of O coverage (from the clean surface in black to the full monolayer of O adatoms in red), at a constant pressure of 1 bar (left). The $T/p_{O_2}$ phase diagram (right) showing the oxidation transition zone (pink) for $W_2N$, separating the pristine (white area) and the fully covered (red) surface regions.

Once the relative stability of the ABC and ABA stackings has been clarified for the scrutinized MXenes, there is still the question regarding the possible effect of the stacking on the chemical reactivity of the MXene surfaces. To answer that question, we studied the atomic N adsorption and molecular $N_2$ adsorption and dissociation, technologically relevant in the Haber-Bosch ammonia synthesis [22], on the eight clean $M_2X$ where ABA stacking is preferred, following the recent study which dealt with these processes on MXenes with ABC stacking [34]. Table 5 reports the $N_2$ adsorption energies, $E_{\mathrm{ads}}^{\mathrm{N_2}}$, the N adatom adsorption energies, $E_{\mathrm{ads}}^{N}$, with respect to ½·$N_2$, the $N_2$ dissociation energy barrier, $E_{\mathrm{b}}^{\mathrm{N_2}}$, and the reaction step energy change, $E_{\mathrm{reaction}}^{\mathrm{N_2 \rightarrow 2N}}$, when occurring either on the ABC or the ABA stacking conformations. The results reveal changes in adsorption energies that can be in some cases negligible, of 0.01 eV for N adsorption on $Mo_2N$ and $W_2N$, to noticeable, of almost 1 eV for $N_2$ adsorption on $Nb_2N$. The

impact on the reaction energy changes ranges between 0.03 and 0.70 eV. Some $N_2$ dissociation energy barriers remained unchanged, while others varied by up to around 0.3 eV. $Nb_2N$ is the only case where the $N_2$ dissociation barrier is found to be higher with ABA than with ABC alignment. Lastly, we calculated the energy barriers for the triple hydrogenation of an N adatom on $W_2N$ to form $NH_3$ for both ABC and ABA stacking. For the ABC-stacked $W_2N$ the calculated values are 1.24, 1.70, and 1.69 eV whereas for the ABA stacking of $W_2N$ these values change to 0.85, 1.21 and 1.72 eV, thus greatly facilitating the first two hydrogenations, reducing the barriers by 0.39 and 0.51 eV, while the third is merely heightened by 0.03 eV. Thus, it appears that the impact of stacking on a reaction profile can be significant, with adsorption strengths changes up to *ca.* 1 eV, and energy barrier changes of up to ~0.3 eV, which can signify changes in the reaction step rate constant of up to three or four orders of magnitude in the temperature range of 400-700 K. Consequently, and to avoid unduly model-biased artifacts in computed results, the use of the correct stacking conformation under working *operando* conditions is strongly advised.

**Table 5.** N and $N_2$ adsorption energies, $E_{\mathrm{ads}}^{N}$ and $E_{\mathrm{ads}}^{\mathrm{N_2}}$, respectively, $N_2$ dissociation energy barriers, $E_{\mathrm{b}}^{\mathrm{N_2}}$, and $\mathrm{N_2} \rightarrow 2\mathrm{N}$ reaction step energy change, $E_{\mathrm{reaction}}^{\mathrm{N_2 \rightarrow 2N}}$, on the $M_2X$ MXenes with preference towards ABA stacking. All values are given in eV and include ZPE corrections.

| MXene | ABC stacking | | | | ABA stacking | | | |
|---|---|---|---|---|---|---|---|---|
| | $E_{\mathrm{ads}}^{N}$ | $E_{\mathrm{ads}}^{\mathrm{N_2}}$ | $E_{\mathrm{b}}^{\mathrm{N_2}}$ | $E_{\mathrm{reaction}}^{\mathrm{N_2 \rightarrow 2N}}$ | $E_{\mathrm{ads}}^{N}$ | $E_{\mathrm{ads}}^{\mathrm{N_2}}$ | $E_{\mathrm{b}}^{\mathrm{N_2}}$ | $E_{\mathrm{reaction}}^{\mathrm{N_2 \rightarrow 2N}}$ |
| $Cr_2C$ | -2.01 | -2.12 | 0.85 | -1.90 | -1.71 | -2.06 | 0.78 | -1.37 |
| $Mo_2C$ | -1.97 | -1.59 | 0.93 | -2.35 | -1.76 | -1.36 | 0.62 | -2.16 |
| $W_2C$ | -1.79 | -1.11 | 0.37 | -2.48 | -1.84 | -1.14 | 0.37 | -2.53 |
| $Nb_2N$ | -2.23 | -1.76 | 0.60 | -2.70 | -2.34 | -2.68 | 0.78 | -2.00 |
| $Ta_2N$ | -2.59 | -2.12 | 0.48 | -3.06 | -2.61 | -2.85 | 0.54 | -2.38 |
| $Cr_2N$ | -1.76 | -1.66 | 0.61 | -1.85 | -1.94 | -1.99 | 0.61 | -1.89 |
| $Mo_2N$ | -2.15 | -1.55 | 0.45 | -2.76 | -2.16 | -1.73 | 0.41 | -2.60 |
| $W_2N$ | -2.26 | -1.34 | 0.28 | -3.19 | -2.25 | -1.27 | 0.18 | -3.22 |

## Conclusions

A first-principles DFT study including dispersion was carried out for a total of 54 MXene 2D transition metal carbide and nitride materials. The analysis of the results reveals that the ABA type of layer stacking is competitive for a number of cases meaning that the MAX-derived ABC stacking cannot be taken as granted. Energetic data reveal that the ABA stacking appears to be more frequent than anticipated and is fostered by the number of the constituent metal *d*

electrons, preferred by nitride instead of carbide MXenes, and favored by the O surface termination. The calculated sliding energy barriers for the conversion of ABC towards ABA reveal very small energy barriers as low as 0.12 eV per formula unit for some MXenes, and higher ones, up to 1.12 eV per formula unit, for thicker $M_3X_2$ and $M_4X_3$ MXenes, in any case, surmountable at high temperature *operando* conditions. On $M_2X$ systems, the adsorption of species or the formation of an O overlayer can be enough to prompt the conversion from ABC towards an ABA stacking. This ABA layer stacking was found to influence the adsorption energies and reaction energy barriers of surface on-going processes, with energetic changes that can vary between a few hundredths of eV to ~1 eV, which can definitely bias the reaction profile, even the reaction step rate constants, by up to three or four orders of magnitude in usual working condition temperatures. To summarize, the present study provides compelling evidence that the atomic layer stacking on MXenes can be different from that expected from the MAX phase precursor for nearly half of the studied MXenes, with several important consequences for the MXene surfaces chemistry and, likely, on physical properties as well which call for further analysis. A careful atomic structure determination is advised rather than assuming that corresponding to the parent MAX phase. Computational models should seriously also consider this issue.

## Acknowledgements

The research carried out at the CICECO – University of Aveiro Institute of Materials, was developed within the scope of the projects UIDB/50011/2020 & UIDP/50011/2020, financed by national funds through the Portuguese *Fundação para a Ciência e a Tecnologia* (FCT/MEC) and co-financed by FEDER under the PT2020 Partnership Agreement. The research carried out at the *Universitat de Barcelona* has been supported by the Spanish MICIUN/FEDER RTI2018-095460-B-I00 and *María de Maeztu* MDM-2017-0767 grants and, in part, by *Generalitat de Catalunya* 2017SGR13 and XRQTC grants. J.D.G. is also thankful to projects CENTRO-01-0145-FEDER-31002 (SILVIA) and HPC-EUROPA3 (INFRAIA-2016-1-730897) supported by the EC Research Innovation Action under the H2020 Programme. F. I. acknowledges additional support from the 2015 ICREA Academia Award for Excellence in University Research.

## References


[1] M. Naguib, M. Kurtoglu, V. Presser, J. Lu, J. Niu, M. Heon, L. Hultman, Y. Gogotsi and M. W. Barsoum, Adv. Mater. **23**, 4248–53 (2011).

[2] M. Naguib and Y. Gogotsi Y, Acc. Chem. Res. **48**, 128-35 (2015).

[3] L. Zhao, B. Dong, S. Li, L. Zhou, L. Lai, Z. Wang, S. Zhao, M. Han, K. Gao, M. Lu, X. Xie, B. Chen, Z. Liu, X. Wang, H. Zhang, H. Li, J. Liu, H. Zhang, X. Huang and W. Huang W, ACS Nano **11**, 5800-07 (2017).

[4] A. Morales-García, A. Fernández-Fernández, F. Viñes and F. Illas, J. Mater. Chem. A **6**, 3381-85 (2018).

[5] I. Persson, J. Halim, H. Lind, T. W. Hansen, J. B. Wagner, L. Å. Näslund, V. Darakchieva, J. Palisaitis, J. Rosen and P. O. Å. Persson, Adv. Mater. **31**, 1805472 (2019).

[6] M. R. Lukatskaya, O. Mashtalir, C. R. Ren, Y. Dall'Agnese, P. Rozier, P. L. Taberna, M. Naguib, P. Simon, M. W. Barsoum and Y. Gogotsi, Science **341**, 1502-5 (2013).

[7] C. Lu, D. Tranca, J. Zhang, F. Rodríguez Hernández, Y. Su, X. Zhuang, F. Zhang, G. Seifert and X. Feng, ACS Nano **11**, 3933-42 (2017).

[8] G. Gao, A. P. O'Mullane and A. Du, ACS Catal. **7**, 494-500 (2017).

[9] L. Ma, L. R. L. Ting, V. Molinari, C. Giordano and B. S. Yeo, J. Mater. Chem. A **3**, 8361-8 (2015).

[10] M. –S. Cao, Y. –Z. Cai, J. –C. Cai, P. He, J. C. Shu, W. Q. Cao and J. Yuan, Chem. Eng. J. **359**, 1265-302 (2019).

[11] M. Alhabeb, K. Maleski, T. S. Mathis, A. Sarycheva, C. B. Hatter, S. Uzun, A. Levitt and Y. Gogotsi, Angew. Chem. Int. Ed. **57**, 5444-8 (2018).

[12] M. Alhabeb, K. Maleski, B. Anasori, P. Lelyukh, L. Clark, S. Sin and Y. Gogotsi, Chem. Mater. **29**, 7633-44 (2017).

[13] O. Mashtalir, M. Naguib, V. N. Mochalin, Y. Dall'Agnese, M. Heon, M. W. Barsoum and Y. Gogotsi, Nat. Commun. **4**, 1716 (2013).

[14] J. Peng, X. Chen, W. J. Ong, X. Zhao and N. Li, Chem **5**, 18–50 (2019).

[15] T. Li, L. Yao, Q. Liu, J. Gu, R. Luo, J. Li, X. Yan, W. Wang, P. Liu, B. Chen, W. Zhang, W. Abbas, R. Naz and D. Zhang, Angew. Chem. Int. Ed. **57**, 6115–9 (2018).

[16] Y. F. Guan, S. Jiang, Y. Cong, J. P. Wang, Z. J. Dong, Q. Zhang, G. M. Yuan, Y. J. Li and X. K. Li, 2D Mater. **7**, 025010 (2020).

[17] G. Deysher, C. E. Shuck, K. Hantanasirisakul, N. C. Frey, A. C. Foucher, K. Maleski, A. Sarycheva, V. B. Shenoy, E. A. Stach, B. Anasori and Y. Gogotsi, ACS Nano **14**, 207–14 (2020).

[18] J. L. Hart, K. Hantanasirisakul, A. C. Lang, B. Anasori, D. Pinto, Y. Pivak, J. Tijn van Omme, S. J. May, Y. Gogotsi and M. L. Taheri, Nat. Comm. **10**, 522 (2019).

[19] M. Shao, Y. Shao, W. Chen, K. L. Ao, R. Tong, Q. Zhu, I. N. Chan, W. F. Ip, X. Shi and H. Pan, Phys. Chem. Chem. Phys. **20**, 14504–12 (2018).

[20] P. Urbankowski, B. Anasori, K. Hantanasirisakul, L. Yang, L. Zhang, B. Haines, S. J. May, S. J. E. Billinge and Y. Gogotsi, Nanoscale **9**, 17722–30 (2017).

[21] H. Lv, W. Wei, P. Zhao, E. Er, B. Huang, Y. Dai and T. Jacob, J. Catal. **378**, 97–103 (2019).

[22] J. W. Erisman, M. A. Sutton, J. Galloway, Z. Klimont and W. Winiwater, Nat. Geosci. **1**, 636–9 (2008).

[23] G. Kresse and J. Furthmüller, Phys. Rev. B **54**, 11169 (1996).

[24] J. P. Perdew, K. Burke and M. Ernzerhof, Phys. Rev. Lett. **77**, 3865 (1996).

[25] S. Grimme, J. Antony, S. Ehrlich and H. Krieg, J. Chem. Phys. **132**, 154104 (2010).

[26] P. E: Blöchl, Phys. Rev. B **50**, 17953 (1994).

[27] N. Zhang, Y. Hong, S. Yazdanparast and M. A. Zaeem, 2D Mater. **5**, 045004 (2018).

[28] M. Kurtoglu, M. Naguib, Y. Gogotsi and M. W. Barsoum, MRS Commun. **2**, 133–7 (2012).

[29] W. Sun, Y. Li, B. Wang, X. Jiang, M. I. Katsnelson, P. Korzhavyi, O. Eriksson and I. Di Marco, Nanoscale **8**, 15753–62 (2016).

[30] H. J. Monkhorst and J. D. Pack, Phys. Rev. B **13**, 5188 (1976).

[31] G. Henkelman and H. Jónsson, J. Chem. Phys. **111**, 7010 (1999).

[32] J. Rogal and K. Reuter, Educational Notes RTO-EN-AVT-142, **2**, 2-1–2-18 (2007).

[33] K. Huber and W. A. Wagner, Work Functions of Metals, in Solid Surface Physics, Springer, Berlin, Heidelberg (1979).

[34] J. D. Gouveia, Á. Morales-García, F. Viñes, J. R. B. Gomes and F. Illas, ACS Catal. **10**, 5049-56 (2020).